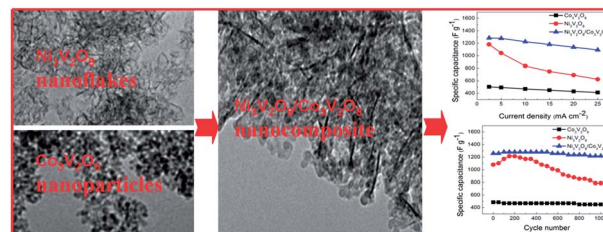


1

## Synthesis and characterization of $M_3V_2O_8$ ( $M = Ni$ or $Co$ ) based nanostructures: a new family of high performance pseudocapacitive materials

Mao-Cheng Liu, Ling-Bin Kong,\* Long Kang, Xiaohong Li, Frank C. Walsh, Man Xing, Chao Lu, Xue-Jing Ma and Yong-Chun Luo

$M_3V_2O_8$  nanostructures are designed and synthesized as new materials for supercapacitors according to their structural characteristics and pseudocapacitive properties; they exhibit superior electrochemical performance to traditional metal oxides.



1

5

10

3

1

5

10

15

Please check this proof carefully. **Our staff will not read it in detail after you have returned it.**

15

Translation errors between word-processor files and typesetting systems can occur so the whole proof needs to be read. Please pay particular attention to: tabulated material; equations; numerical data; figures and graphics; and references. If you have not already indicated the corresponding author(s) please mark their name(s) with an asterisk. Please e-mail a list of corrections or the PDF with electronic notes attached - do not change the text within the PDF file or send a revised manuscript. Corrections at this stage should be minor and not involve extensive changes. All corrections must be sent at the same time.

20

20

25

**Please bear in mind that minor layout improvements, e.g. in line breaking, table widths and graphic placement, are routinely applied to the final version.**

25

We will publish articles on the web as soon as possible after receiving your corrections; **no late corrections will be made.**

30

Please return your **final** corrections, where possible within **48 hours** of receipt by e-mail to: materialsA@rsc.org

30

35

35

40

40

45

45

50

50

# Queries for the attention of the authors




Journal: Journal of Materials Chemistry A

Paper: c4ta00582a

Title: Synthesis and characterization of  $M_3V_2O_8$  ( $M = Ni$  or  $Co$ ) based nanostructures: a new family of high performance pseudocapacitive materials

Editor's queries are marked like this... **1**, and for your convenience line numbers are inserted like this... 5

Please ensure that all queries are answered when returning your proof corrections so that publication of your article is not delayed.

| Query Reference | Query   | Remarks   |
|-----------------|---|---|
| 1               | For your information: You can cite this article before you receive notification of the page numbers by using the following format: (authors), J. Mater. Chem. A, (year), DOI: 10.1039/c4ta00582a.               |  |
| 2               | Please carefully check the spelling of all author names. This is important for the correct indexing and future citation of your article. No late corrections can be made.                                       |  |
| 3               | Please check that the GA text fits within the allocated space indicated on the front page of the proof. If the entry does not fit between the two horizontal lines, then please trim the text and/or the title. |  |



# Synthesis and characterization of $M_3V_2O_8$ ( $M = Ni$ or $Co$ ) based nanostructures: a new family of high performance pseudocapacitive materials†

Mao-Cheng Liu,<sup>a</sup> Ling-Bin Kong,<sup>\*ab</sup> Long Kang,<sup>b</sup> Xiaohong Li,<sup>c</sup> Frank C. Walsh,<sup>c</sup> Man Xing,<sup>a</sup> Chao Lu,<sup>a</sup> Xue-Jing Ma<sup>a</sup> and Yong-Chun Luo<sup>b</sup>

Binary metal oxides have recently attracted extensive attention from researchers in the energy storage field due to their multiple oxidation states and high energy density. In the present work,  $Ni_3V_2O_8$ ,  $Co_3V_2O_8$ , and the  $Ni_3V_2O_8/Co_3V_2O_8$  nanocomposite are designed and synthesized as a new class of high performance electrode material for supercapacitors.  $Ni_3V_2O_8$  and  $Co_3V_2O_8$  show a structure comprising nanoflakes and nanoparticles, respectively. The  $Ni_3V_2O_8/Co_3V_2O_8$  nanocomposite is prepared by growing  $Co_3V_2O_8$  nanoparticles on the surface of  $Ni_3V_2O_8$  nanoflakes. The composite inherits the structural characteristics and combines the pseudocapacitive benefits of both  $Ni_3V_2O_8$  and  $Co_3V_2O_8$ , showing higher specific capacitance than  $Co_3V_2O_8$  and superior rate capability as well as better cycle stability to  $Ni_3V_2O_8$ . The dependence of pseudocapacitive properties of the  $Ni_3V_2O_8/Co_3V_2O_8$  nanocomposite on the Ni/Co mass ratio is also investigated, indicating that the high specific capacitance of the composite is contributed by  $Ni_3V_2O_8$ , while its excellent rate capability and cycle stability can be attributed to the  $Co_3V_2O_8$  component.

Received 2nd February 2014  
Accepted 12th February 2014

DOI: 10.1039/c4ta00582a

www.rsc.org/MaterialsA

## 1. Introduction

Supercapacitors are electrochemical devices that store and release energy at a high rate (in seconds) with a high power density ( $10 \text{ kW kg}^{-1}$ ) and long cycle life; they have potential applications in electronic devices, hybrid electric vehicles and military devices.<sup>1–6</sup> For high power applications, however, a major disadvantage is that they have an unsatisfactory energy density (typically,  $4–5 \text{ W h kg}^{-1}$  for those based on porous activated carbon) compared to batteries (*e.g.*,  $26–34 \text{ W h kg}^{-1}$  for lead acid batteries).<sup>7,8</sup> Therefore, improving the energy density of supercapacitors while maintaining their high power density and long cycle life has been the key driving force in developing future supercapacitors.<sup>9,10</sup> Generally, transition metal oxides and conducting polymers deliver higher energy density than carbon materials due to their pseudocapacitive characteristics. As pseudocapacitive materials, multiple oxidation states/structures

will enable rich redox reactions for the improvement of capacitance.<sup>11–13</sup> Transition metal oxides are such a class of materials and have attracted considerable attention.<sup>14–16</sup>

Among transition metal oxides, mixed metal oxides<sup>17–19</sup> and binary metal oxides<sup>20–22</sup> possess multiple oxidation states that enable multiple redox reactions; they have been reported to exhibit a higher supercapacitive performance than single component metal oxides, and seem to be some of the most promising and low cost materials for pseudocapacitors. For example, spinel nickel cobaltite aerogels,<sup>14</sup> urchin-like  $NiCo_2O_4$  nanostructures,<sup>23</sup>  $NiCo_2O_4$ -SWCNT nanocomposites,<sup>24</sup> nickel cobaltite/carbon aerogel composites,<sup>25</sup> mesoporous  $NiCo_2O_4$  nanosheets on conductive substrates<sup>26</sup> and hierarchical porous  $NiCo_2O_4$  nanowires<sup>27</sup> have been reported as new electrode materials for supercapacitors and shown excellent pseudocapacitive properties, indicating that the design and synthesis of binary metal oxides is an effective way to improve pseudocapacitance of the metal oxides. Our previous studies on the binary metal oxides  $NiCo_2O_4$ ,<sup>20</sup>  $NiMoO_4$ ,<sup>28</sup> and  $CoMoO_4$ <sup>29,30</sup> also suggest that they exhibit higher pseudocapacitance than single component metal oxides. Thus, it appears that binary metal oxides could be a material of choice for pseudocapacitors. However, these studies are only focused on the design and realisation of the unique microstructure; no generation mechanism of pseudocapacitance is involved for binary metal oxides, though it is important for the design of new binary metal oxides with higher pseudocapacitance.

<sup>a</sup>State Key Laboratory of Advanced Processing and Recycling of Nonferrous Metals, Lanzhou University of Technology, Lanzhou 730050, PR China. E-mail: konglb@lut.cn; Fax: +86-931-2976578; Tel: +86-931-2976579

<sup>b</sup>School of Materials Science and Engineering, Lanzhou University of Technology, Lanzhou 730050, PR China

<sup>c</sup>Electrochemical Engineering Laboratory, Energy Technology Research Group, Faculty of Engineering and the Environment, University of Southampton, Highfield, Southampton, SO17 1BJ, UK

† Electronic supplementary information (ESI) available. See DOI: 10.1039/c4ta00582a

In order to explore the contribution of both metal elements to the pseudocapacitance of binary metal oxides, the binary metal oxides ( $A_xB_yO_z$ ) are classified as  $AB_2O_4$ ,  $ABO_4$ , and  $A_3B_2O_8$  types in our studies, where A and B represent the metal elements having low and high oxidation states, respectively. Detailed studies on these materials indicate that the element A plays a significant role in the generation of pseudocapacitance, while B has a minor influence on the capacitances of the binary metal oxides (see Fig. S1† and the discussion). This means that binary metal oxides ( $A_3B_2O_8$  type) with a higher atom proportion of A would exhibit a higher pseudocapacitance. This concept inspired us to design and synthesize an  $A_3B_2O_8$  type binary metal oxide having a high content of A to achieve excellent properties, where B is a pentavalent metal ion. In the periodic table of elements, only vanadium is such an element that can serve as a B metal element (pentavalent vanadium) and form an  $A_3B_2O_8$  type binary metal oxide. Interestingly, it is reported that  $A_3B_2O_8$  ( $M = Ni$  or  $Co$ ) has a crystalline structure in a Kagome-staircase geometry and shows interesting magnetic behavior as well as excellent catalytic activities due to its unique structural feature.<sup>31–34</sup> It is an important kind of binary metal oxide with a higher A/B ratio (3 : 2) than  $MMoO_4$  (1 : 1) and  $MCo_2O_4$  (1 : 2), where M represents Ni or Co. However, the supercapacitance of the  $M_3V_2O_8$  based materials has not yet been investigated and reported.

In this work, we report  $M_3V_2O_8$  ( $M = Ni$  or  $Co$ ) materials as a new family of high performance pseudocapacitive materials, and synthesize them by a simple and facile chemical coprecipitation technique. The rate capability and cycle stability of  $Co_3V_2O_8$  are excellent, while  $Ni_3V_2O_8$  exhibits high specific capacitance. Based on these studies, to combine the advantages of both  $Ni_3V_2O_8$  and  $Co_3V_2O_8$ , a hybrid  $Ni_3V_2O_8/Co_3V_2O_8$  nanocomposite was designed and synthesised by growing  $Co_3V_2O_8$  nanoparticles on  $Ni_3V_2O_8$  nanoflakes; the resultant composite provides an excellent combination of the properties of  $Co_3V_2O_8$  and  $Ni_3V_2O_8$  and exhibits superior electrochemical performance including an ultrahigh specific capacitance, excellent rate capability, and exceptional cycle stability.

## 2. Experimental section

### 2.1 Synthesis of materials

All chemical reagents were analytical grade and purchased from Sinopharm Chemical Reagent Co. Ltd. In a typical synthesis of  $Ni_3V_2O_8$  and  $Co_3V_2O_8$ , 5 mmol of  $NiCl_2 \cdot 6H_2O$  and  $CoCl_2 \cdot 6H_2O$  were dissolved in 30 ml distilled water and stirred at 70 °C. 30 ml distilled water containing 6 mmol of  $Na_3VO_4 \cdot 12H_2O$  was added dropwise and the resulting suspension was stirred at 70 °C for 4 h.  $Ni_3V_2O_8/Co_3V_2O_8$  composites were prepared by the same method using  $Ni_3V_2O_8$  as the backbone material. Typically, 5 mmol of  $NiCl_2 \cdot 6H_2O$  was dissolved in 30 ml distilled water and stirred at 70 °C. 60 ml distilled water containing 12 mmol of  $Na_3VO_4 \cdot 12H_2O$  was added dropwise and the resulting suspension was stirred at 70 °C for 4 h. Finally, 20 ml distilled water containing 5 mmol of  $CoCl_2 \cdot 6H_2O$  was added dropwise and stirred for an additional 4 h. The resultant solids

were filtered, washed with a copious amount of distilled water and dried at 80 °C for 12 h.

### 2.2 Structural characterization

The microstructure and morphology of the materials were characterized using a transmission electron microscope (TEM, JEOL, JEM-2010, Japan) and a field emission scanning electron microscope (SEM, JEOL, JSM-6701F, Japan). Crystallite structures were determined by X-ray diffraction (XRD) using a Rigaku D/MAX 2400 diffractometer (Japan) with Cu K $\alpha$  radiation ( $\lambda = 1.5418 \text{ \AA}$ ) operating at 40 kV and 60 mA. The surface areas were investigated by volumetric nitrogen adsorption/desorption experiments (ASAP 2020) using a BJH algorithm for extraction of pore data.

### 2.3 Preparation of the electrode

80 wt% of the active material was mixed with 7.5 wt% of acetyle black and 7.5 wt% of conducting graphite in an agate mortar until a homogeneous black powder was obtained. 5 wt% of poly(tetrafluoroethylene) was added together with a few drops of ethanol. The resulting paste was pressed at 10 MPa into an open-cell nickel foam (ChangSha Lyrun New Material Co. Ltd, grade 90 PPI (pores per linear inch), 2 mm thick), then dried at 80 °C for 12 h. Each electrode contained 4 mg of the electroactive material and had a geometric surface area of 1 cm<sup>2</sup>.

### 2.4 Electrochemical measurements

The electrochemical measurements were carried out using a conventional three-electrode system with an aqueous solution (electrolyte: 2 M KOH). A platinum sheet electrode (1.5 cm  $\times$  1.5 cm) with a surface area of 2.25 cm<sup>2</sup> was used as the counter electrode and a saturated calomel electrode (SCE) served as the reference electrode. The cyclic voltammetry (CV), charge-discharge tests, and electrochemical impedance spectroscopy (EIS) measurements were performed using an electrochemical workstation (CHI660C, Shanghai, China). The EIS plots were obtained in the frequency range from 100 kHz to 0.1 Hz at the open-circuit potential with a sinusoidal ac perturbation of 5 mV. The cycling performance was tested using a CT2001A battery program controlling test system (China-Land Com. Ltd). The specific capacitance of the electrodes was calculated from the following equation:

$$C_m = \frac{C}{m} = \frac{I \times \Delta t}{\Delta V \times m} \quad (1)$$

where  $C_m$  (F g<sup>-1</sup>) is the specific capacitance,  $C$  is the total capacitance,  $I$  (A) is the discharge current,  $\Delta t$  (s) is the discharge time,  $\Delta V$  (V) represents the potential drop during discharge, and  $m$  (g) is the mass of the active material.

## 3. Results and discussion

The crystallographic phases of  $Ni_3V_2O_8$ ,  $Co_3V_2O_8$ , and the  $Ni_3V_2O_8/Co_3V_2O_8$  nanocomposite determined by XRD are shown in Fig. 1.

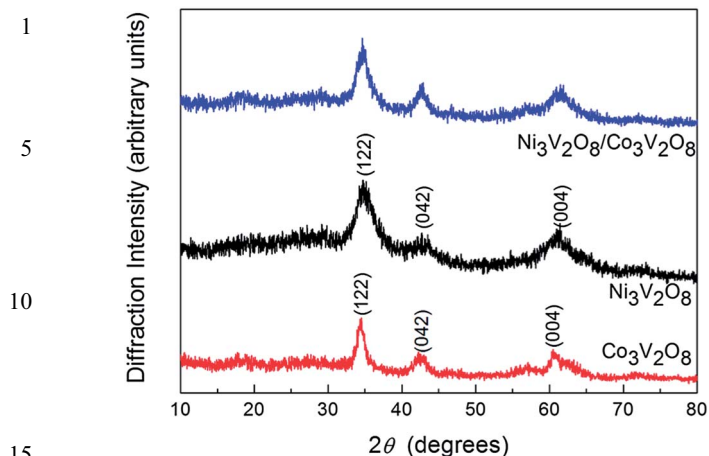


Fig. 1 XRD patterns of  $\text{Ni}_3\text{V}_2\text{O}_8$ ,  $\text{Co}_3\text{V}_2\text{O}_8$ , and the  $\text{Ni}_3\text{V}_2\text{O}_8/\text{Co}_3\text{V}_2\text{O}_8$  nanocomposite with a Ni/Co molar ratio of 1 : 1.

The patterns of the components  $\text{Ni}_3\text{V}_2\text{O}_8$  and  $\text{Co}_3\text{V}_2\text{O}_8$  are in good agreement with the standard patterns for  $\text{Ni}_3\text{V}_2\text{O}_8$  (PDF 74-1484) and  $\text{Co}_3\text{V}_2\text{O}_8$  (PDF 74-1486); typical diffraction peaks of  $\text{Ni}_3\text{V}_2\text{O}_8$  and  $\text{Co}_3\text{V}_2\text{O}_8$  are apparent. The pattern of the  $\text{Ni}_3\text{V}_2\text{O}_8/\text{Co}_3\text{V}_2\text{O}_8$  nanocomposite contains the diffraction peaks of both  $\text{Ni}_3\text{V}_2\text{O}_8$  and  $\text{Co}_3\text{V}_2\text{O}_8$ . Because  $\text{Ni}_3\text{V}_2\text{O}_8$  (PDF 74-1484:  $a = 8.24 \text{ \AA}$ ,  $b = 11.38 \text{ \AA}$ ,  $c = 5.91 \text{ \AA}$ ) has a similar crystal lattice parameter to  $\text{Co}_3\text{V}_2\text{O}_8$  (PDF 74-1486:  $a = 8.30 \text{ \AA}$ ,  $b = 11.50 \text{ \AA}$ ,  $c = 6.03 \text{ \AA}$ ), lattice matching between  $\text{Ni}_3\text{V}_2\text{O}_8$  and  $\text{Co}_3\text{V}_2\text{O}_8$  can readily occur and the pattern of the composite is almost consistent with that of a  $\text{Ni}_3\text{V}_2\text{O}_8$  and  $\text{Co}_3\text{V}_2\text{O}_8$  mixture. The weak diffraction

intensity of the samples reveals a poor crystallization or an amorphous form of the  $\text{M}_3\text{V}_2\text{O}_8$  based materials prepared by a facile chemical co-precipitation technique. This is favorable for improving the capacitance since a material having poor crystallinity may result in more transportation channels than a highly crystalline one.<sup>35</sup> X-ray photoelectron spectroscopy (XPS) was also carried out to determine the materials, as shown in Fig. S2;†  $\text{Ni}^{2+}$ ,  $\text{Co}^{2+}$ , and  $\text{V}^{5+}$  were revealed to be present in  $\text{M}_3\text{V}_2\text{O}_8$  based materials, agreeing well with the results of the XRD.

Fig. 2a and b show the TEM images of the  $\text{Ni}_3\text{V}_2\text{O}_8$  and  $\text{Co}_3\text{V}_2\text{O}_8$  samples. A nanoflake and a nanoparticle structure are observed for  $\text{Ni}_3\text{V}_2\text{O}_8$  and  $\text{Co}_3\text{V}_2\text{O}_8$ , respectively. For preparation of the  $\text{Ni}_3\text{V}_2\text{O}_8/\text{Co}_3\text{V}_2\text{O}_8$  nanocomposite, we consider that the flake-like structure of  $\text{Ni}_3\text{V}_2\text{O}_8$  is more suitable to serve as the skeleton structure for growing  $\text{Co}_3\text{V}_2\text{O}_8$  nanoparticles because of its larger surface area. The microstructure of the prepared  $\text{Ni}_3\text{V}_2\text{O}_8/\text{Co}_3\text{V}_2\text{O}_8$  nanocomposite is shown in Fig. 2c and d; it is obvious that the  $\text{Ni}_3\text{V}_2\text{O}_8$  nanoflakes are serving as the 'substrate' and the  $\text{Co}_3\text{V}_2\text{O}_8$  nanoparticles are growing on the surface of  $\text{Ni}_3\text{V}_2\text{O}_8$  nanoflakes. Fig. 2e shows the surface morphology of the composite, as the  $\text{Ni}_3\text{V}_2\text{O}_8$  nanoflakes are coated by  $\text{Co}_3\text{V}_2\text{O}_8$  nanoparticles; only nanoparticles are observed in the SEM image. The growth of  $\text{Co}_3\text{V}_2\text{O}_8$  nanoparticles on the surface of  $\text{Ni}_3\text{V}_2\text{O}_8$  nanoflakes will not only prevent the agglomeration of the  $\text{Co}_3\text{V}_2\text{O}_8$  nanoparticles, but also avoid the crumple and the shrink of the  $\text{Ni}_3\text{V}_2\text{O}_8$  nanoflakes in the later drying process after synthesis. The nanoflake and nanoparticle structure characteristics of  $\text{Ni}_3\text{V}_2\text{O}_8$  and  $\text{Co}_3\text{V}_2\text{O}_8$  are perfectly retained in the composite; this helps achieve a

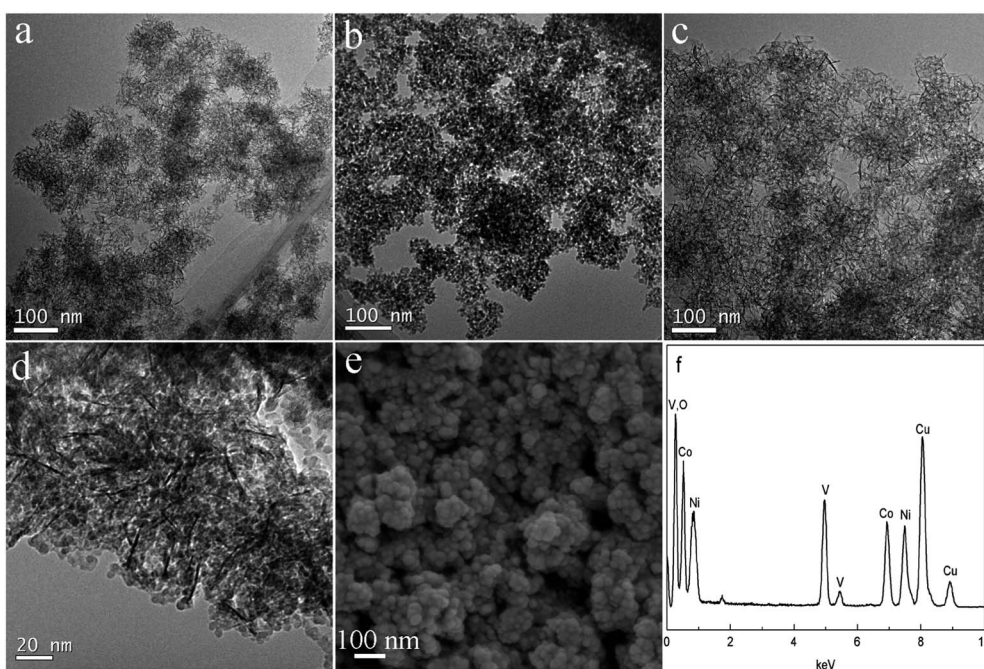


Fig. 2 TEM images of (a)  $\text{Ni}_3\text{V}_2\text{O}_8$  nanoflakes, (b)  $\text{Co}_3\text{V}_2\text{O}_8$  nanoparticles, and (c)  $\text{Ni}_3\text{V}_2\text{O}_8/\text{Co}_3\text{V}_2\text{O}_8$  nanocomposite with a Ni/Co molar ratio of 1 : 1. (d) HRTEM and (e) SEM images of the  $\text{Ni}_3\text{V}_2\text{O}_8/\text{Co}_3\text{V}_2\text{O}_8$  nanocomposite. (f) EDS spectrum of the  $\text{Ni}_3\text{V}_2\text{O}_8/\text{Co}_3\text{V}_2\text{O}_8$  nanocomposite with a Ni/Co molar ratio of 1 : 1.

robust structure in the nanocomposite materials. Energy dispersive spectroscopy (EDS) microanalysis reveals that the composite consists of Co, Ni, V, and O elements, while the Cu comes from the copper grid. The results are consistent with the XRD analysis. The composite is made of  $\text{Ni}_3\text{V}_2\text{O}_8$  and  $\text{Co}_3\text{V}_2\text{O}_8$ .

Fig. 3a shows the  $\text{N}_2$  adsorption/desorption isotherms of  $\text{Ni}_3\text{V}_2\text{O}_8$ ,  $\text{Co}_3\text{V}_2\text{O}_8$ , and the  $\text{Ni}_3\text{V}_2\text{O}_8/\text{Co}_3\text{V}_2\text{O}_8$  nanocomposite. All of the isotherms exhibit the characteristics of type IV isotherms with hysteresis loops, indicating a typical mesoporous structure.<sup>36,37</sup> Fig. 3b displays the corresponding pore size distribution of the three samples. All the samples exhibit a distribution in the mesopore region. The relevant structural parameters derived from the isotherms are summarized in Table 1. The specific surface area of  $\text{Ni}_3\text{V}_2\text{O}_8$  is higher and the pore volume is lower than those in  $\text{Co}_3\text{V}_2\text{O}_8$  because the nanoflake structure of  $\text{Ni}_3\text{V}_2\text{O}_8$  possesses a large surface area, while the nanoparticle structure of  $\text{Co}_3\text{V}_2\text{O}_8$  shows a higher pore volume. The  $\text{Ni}_3\text{V}_2\text{O}_8/\text{Co}_3\text{V}_2\text{O}_8$  nanocomposite not only inherited the high surface area of  $\text{Ni}_3\text{V}_2\text{O}_8$ , but also achieved a high pore volume by the coating of  $\text{Co}_3\text{V}_2\text{O}_8$  nanoparticles. The combination of the structural advantages of both  $\text{Ni}_3\text{V}_2\text{O}_8$  and  $\text{Co}_3\text{V}_2\text{O}_8$  is a key for the success of the present structural design. Not only does the mesoporous structure of the composite favor the fuller extent immersion of the electrolyte by increased pore volume but also provides a higher reaction surface area by retaining the original advantageous structural features of the  $\text{Ni}_3\text{V}_2\text{O}_8$  nanoflakes.

To evaluate the electrochemical properties of the  $\text{Ni}_3\text{V}_2\text{O}_8$  and  $\text{Co}_3\text{V}_2\text{O}_8$  electrodes, the cyclic voltammetry (CV) curves and charge-discharge curves were measured (see Fig. S3† and the discussion). The corresponding specific capacitances calculated from the discharge curves are shown in Fig. 4a;  $\text{Ni}_3\text{V}_2\text{O}_8$  exhibits a higher specific capacitance ( $1181 \text{ F g}^{-1}$ ) than  $\text{Co}_3\text{V}_2\text{O}_8$  ( $505 \text{ F g}^{-1}$ ) at a current density of  $0.625 \text{ A g}^{-1}$ . However, only 52.9% of this value was retained for the  $\text{Ni}_3\text{V}_2\text{O}_8$  electrode at a current density of  $6.25 \text{ A g}^{-1}$ , which is lower than that of 81.8% for  $\text{Co}_3\text{V}_2\text{O}_8$ . However, the specific capacitances of  $\text{A}_3\text{B}_2\text{O}_8$  type binary metal oxides are higher than those of  $\text{AB}_2\text{O}_4$  and  $\text{ABO}_4$  types; this means that binary metal oxides with a higher atom proportion of A exhibit a higher pseudocapacitance. The cycling data shown in Fig. 4b reveal that though the specific

capacitance of  $\text{Ni}_3\text{V}_2\text{O}_8$  is increased over the first 200 cycles due to complete activation of the active materials,<sup>38,39</sup> only 73% of the capacitance was retained after 1000 cycles. Interestingly, the  $\text{Co}_3\text{V}_2\text{O}_8$  electrode exhibits excellent cycle stability with only 7.4% reduction of capacitance after 1000 cycles. The results indicate that the  $\text{Ni}_3\text{V}_2\text{O}_8$  electrode possesses a high specific capacitance, but its rate capability and cycle stability are inferior and need further improvement. Conversely,  $\text{Co}_3\text{V}_2\text{O}_8$  exhibits excellent rate capability and cycle stability, while its specific capacitance is lower than that of most reported oxides.

Although the specific capacitance of  $\text{Ni}_3\text{V}_2\text{O}_8$  is very high, and the rate capability as well as cycle stability of  $\text{Co}_3\text{V}_2\text{O}_8$  is excellent, it is still difficult to obtain a  $\text{Ni}_3\text{V}_2\text{O}_8$  or  $\text{Co}_3\text{V}_2\text{O}_8$  material combining high specific capacitance, excellent rate capability, and good cycle stability. Studies on  $\text{MnMoO}_4/\text{CoMoO}_4$  heterostructured nanowires<sup>40</sup> and  $\text{CoMoO}_4\text{-NiMoO}_4 \cdot x\text{H}_2\text{O}$  bundles<sup>41</sup> indicate that the composite can combine the pseudo-capacitive advantages of both single components to some extent. However, the sizes of  $\text{MnMoO}_4/\text{CoMoO}_4$  and  $\text{CoMoO}_4\text{-NiMoO}_4 \cdot x\text{H}_2\text{O}$  particles are several microns; this may introduce limited improvements in the capacitance. In order to combine the advantages of both  $\text{Ni}_3\text{V}_2\text{O}_8$  and  $\text{Co}_3\text{V}_2\text{O}_8$ , the nanocomposite  $\text{Ni}_3\text{V}_2\text{O}_8/\text{Co}_3\text{V}_2\text{O}_8$  was prepared by coating  $\text{Co}_3\text{V}_2\text{O}_8$  nanoparticles on  $\text{Ni}_3\text{V}_2\text{O}_8$  nanoflakes. Electrochemical impedance spectroscopy (Fig. S4†) shows that the  $\text{Ni}_3\text{V}_2\text{O}_8/\text{Co}_3\text{V}_2\text{O}_8$  nanocomposite has lower charge transfer resistance and ion diffusion resistance than  $\text{Ni}_3\text{V}_2\text{O}_8$ , which are beneficial to the rate capability.

Cyclic voltammetry has been carried out to give an estimate of the active surface area of materials used for the electrochemical reactions. Fig. 5a shows CV curves of the composite electrode at

Table 1 Structural parameters of  $\text{Ni}_3\text{V}_2\text{O}_8$ ,  $\text{Co}_3\text{V}_2\text{O}_8$ , and the  $\text{Ni}_3\text{V}_2\text{O}_8/\text{Co}_3\text{V}_2\text{O}_8$  composite with a Ni/Co molar ratio of 1 : 1

| Samples   | BET specific surface area ( $\text{m}^2 \text{ g}^{-1}$ ) | BJH specific pore volume ( $\text{cm}^3 \text{ g}^{-1}$ ) | BJH pore size (nm) |
|---|---|---|--------------------|
| $\text{Ni}_3\text{V}_2\text{O}_8$                                 | 210.9   | 0.11  | 4.4                |
| $\text{Co}_3\text{V}_2\text{O}_8$                                 | 146.4   | 0.24  | 7.8                |
| $\text{Ni}_3\text{V}_2\text{O}_8/\text{Co}_3\text{V}_2\text{O}_8$ | 208.6   | 0.18  | 4.4                |

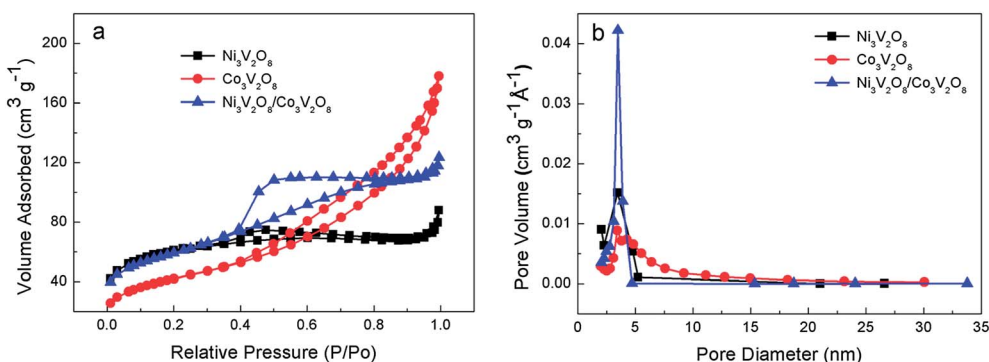


Fig. 3 (a)  $\text{N}_2$  adsorption/desorption isotherms and (b) pore size distribution curves of  $\text{Ni}_3\text{V}_2\text{O}_8$ ,  $\text{Co}_3\text{V}_2\text{O}_8$ , and the  $\text{Ni}_3\text{V}_2\text{O}_8/\text{Co}_3\text{V}_2\text{O}_8$  composite with a Ni/Co molar ratio of 1 : 1.

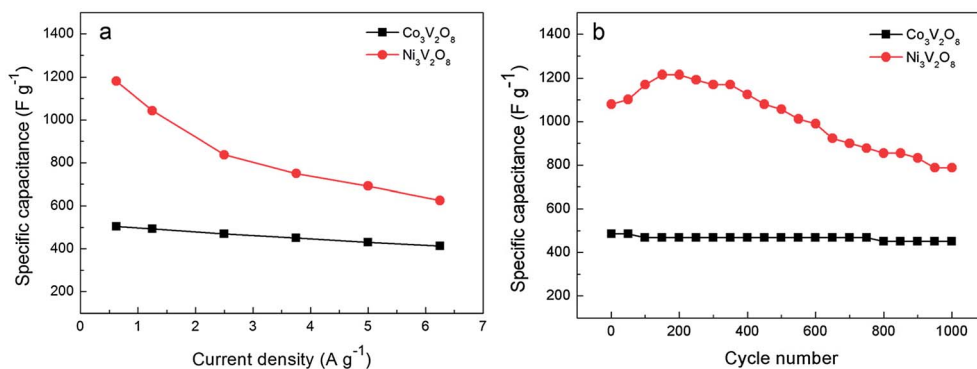


Fig. 4 (a) Specific capacitances of Ni<sub>3</sub>V<sub>2</sub>O<sub>8</sub> and Co<sub>3</sub>V<sub>2</sub>O<sub>8</sub> electrodes at controlled current densities. (b) Cycling performance of Ni<sub>3</sub>V<sub>2</sub>O<sub>8</sub> and Co<sub>3</sub>V<sub>2</sub>O<sub>8</sub> electrodes at a current density of 1.25 A g<sup>-1</sup>.

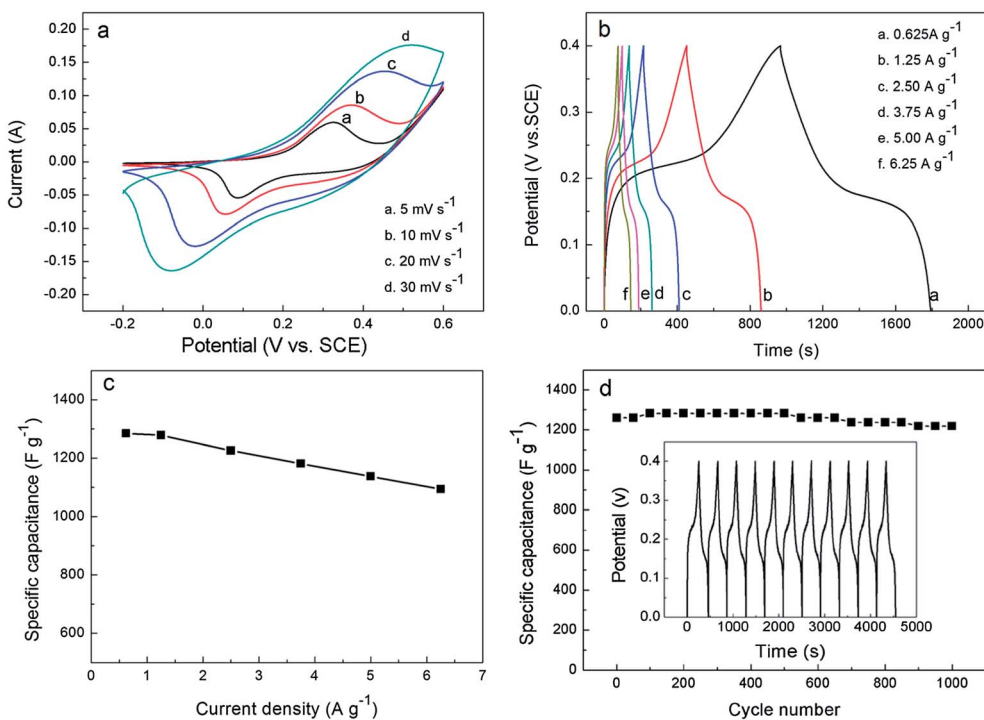


Fig. 5 Electrochemical characterizations of the Ni<sub>3</sub>V<sub>2</sub>O<sub>8</sub>/Co<sub>3</sub>V<sub>2</sub>O<sub>8</sub> composite with a Ni/Co molar ratio of 1 : 1. (a) CV curves at different scan rates. (b) Charge–discharge curves and (c) specific capacitance at controlled current densities. (d) Cycling performance at a current density of 1.25 A g<sup>-1</sup>.

various sweep rates; a pair of redox peaks is visible in each scan. The charges associated with the anodic and cathodic peaks are equal and the peak current densities are proportional to the potential scan rate. From the Pourbaix diagram of Ni, Co and V (shown in Fig. S5<sup>†</sup>), it can be seen that V does not participate in any redox reaction; the capacitance of Ni<sub>3</sub>V<sub>2</sub>O<sub>8</sub>/Co<sub>3</sub>V<sub>2</sub>O<sub>8</sub> is contributed by Ni and Co. Therefore, the redox peaks are associated with surface conversion between metal oxides *e.g.* M(OH)<sub>2</sub> and MOOH,<sup>42–45</sup> as expressed in eqn (2).



The shape of the peaks and the charge balance between total anodic and total cathodic charges confirm that the

electrochemistry is reversible and occurring within a surface layer. To understand the rate capability and to calculate the specific capacitance of the composite, constant-current charge–discharge measurements were performed at various current densities, as shown in Fig. 5b. The calculated specific capacitance of the composite (shown in Fig. 5c) is 1284 F g<sup>-1</sup> at a current density of 0.625 A g<sup>-1</sup> and 85.1% of this value is retained at 6.25 A g<sup>-1</sup>; it is higher than 52.9% and 81.8% of the Ni<sub>3</sub>V<sub>2</sub>O<sub>8</sub> and Co<sub>3</sub>V<sub>2</sub>O<sub>8</sub> single component electrodes. The high specific capacitance and excellent rate capability of the composite are attributed to three contributions. First, it is ascribed to the unique microstructure consisting of Co<sub>3</sub>V<sub>2</sub>O<sub>8</sub> nanoparticles coated on Ni<sub>3</sub>V<sub>2</sub>O<sub>8</sub> nanoflakes, which provides a large surface area for Faraday reactions and enhances the kinetics of ion and

electron transport inside the active materials. Second, it is due to the feasible oxidation states contributed by both  $\text{Co}_3\text{V}_2\text{O}_8$  and  $\text{Ni}_3\text{V}_2\text{O}_8$  components. Third, it can be reasonably attributed to the synergistic effects between  $\text{Co}_3\text{V}_2\text{O}_8$  and  $\text{Ni}_3\text{V}_2\text{O}_8$ . The cycling performance of the composite is recorded as shown in Fig. 5d. After 1000 times of continuous cycling at a current density of  $1.25 \text{ A g}^{-1}$ , 96.7% of the capacitance was retained which is also higher than that of  $\text{Co}_3\text{V}_2\text{O}_8$  (92.6%) and  $\text{Ni}_3\text{V}_2\text{O}_8$  (73.0%). We consider that the excellent cycling stability of the composite is mainly due to the stable microstructure and surface morphology during the charge-discharge process (see Fig. S6†). This means that the composite combines the advantages of the high specific capacitance of  $\text{Ni}_3\text{V}_2\text{O}_8$  and excellent rate capability as well as remarkable stability of  $\text{Co}_3\text{V}_2\text{O}_8$ . This performance is remarkable compared with recently reported  $\text{V}_2\text{O}_5$ ,<sup>46,47</sup>  $\text{NiO}$ ,<sup>48,49</sup>  $\text{MnMoO}_4/\text{CoMoO}_4$  heterostructured nanowires,<sup>40</sup>  $\text{CoMoO}_4\text{-NiMoO}_4 \cdot x\text{H}_2\text{O}$  bundles,<sup>41</sup>  $\text{Co}_3\text{O}_4$  nanowire@ $\text{MnO}_2$  ultrathin nanosheet core-shell arrays,<sup>50</sup>  $\text{V}_2\text{O}_5\text{-TiO}_2$  nanotube arrays,<sup>51</sup> and  $\text{H-TiO}_2/\text{MnO}_2/\text{H-TiO}_2/\text{C}$  core-shell nanowires.<sup>52</sup> The prepared  $\text{Ni}_3\text{V}_2\text{O}_8/\text{Co}_3\text{V}_2\text{O}_8$  nanocomposite shows high specific capacitance and excellent rate capability as well as outstanding cycle stability; considering that the specific capacitance, rate capability, and the cycle stability are three of the most important characteristics for high-performance

supercapacitors, the  $\text{Ni}_3\text{V}_2\text{O}_8/\text{Co}_3\text{V}_2\text{O}_8$  nanocomposite is a promising material for supercapacitors.

In order to determine the contribution of both  $\text{Co}_3\text{V}_2\text{O}_8$  and  $\text{Ni}_3\text{V}_2\text{O}_8$  components to the electrochemical properties of the  $\text{Ni}_3\text{V}_2\text{O}_8/\text{Co}_3\text{V}_2\text{O}_8$  composite, CV curves of  $\text{Ni}_3\text{V}_2\text{O}_8$ ,  $\text{Co}_3\text{V}_2\text{O}_8$ , and  $\text{Ni}_3\text{V}_2\text{O}_8/\text{Co}_3\text{V}_2\text{O}_8$  were recorded at a scan rate of  $20 \text{ mV s}^{-1}$ , as shown in Fig. 6a. Though each CV curve shows redox peaks, the charges associated with the anodic and cathodic peaks are different from each other. The charges associated with the redox peaks of  $\text{Co}_3\text{V}_2\text{O}_8$  are equably distributed in the whole scan potential window, while those of  $\text{Ni}_3\text{V}_2\text{O}_8$  are almost centered on the redox peaks. This indicates that the faradaic reactions of  $\text{Co}_3\text{V}_2\text{O}_8$  can take place in the whole potential window, but those of  $\text{Ni}_3\text{V}_2\text{O}_8$  can only occur around redox peaks. The charges associated with the anodic and cathodic peaks of the  $\text{Ni}_3\text{V}_2\text{O}_8/\text{Co}_3\text{V}_2\text{O}_8$  composite, as compared with those of  $\text{Ni}_3\text{V}_2\text{O}_8$ , show an obvious increase on the reverse cathodic scan. We consider that this increased charge is mainly contributed by the  $\text{Co}_3\text{V}_2\text{O}_8$  component. This means that both  $\text{Co}_3\text{V}_2\text{O}_8$  and  $\text{Ni}_3\text{V}_2\text{O}_8$  components are favorable to improve the supercapacitive performance of the  $\text{Ni}_3\text{V}_2\text{O}_8/\text{Co}_3\text{V}_2\text{O}_8$  composite. Fig. 6b shows the dependence of the specific capacitances on Ni/Co molar ratios in the  $\text{Ni}_3\text{V}_2\text{O}_8/\text{Co}_3\text{V}_2\text{O}_8$  composites. The specific capacitances of the composites increased at higher Ni/Co molar ratios

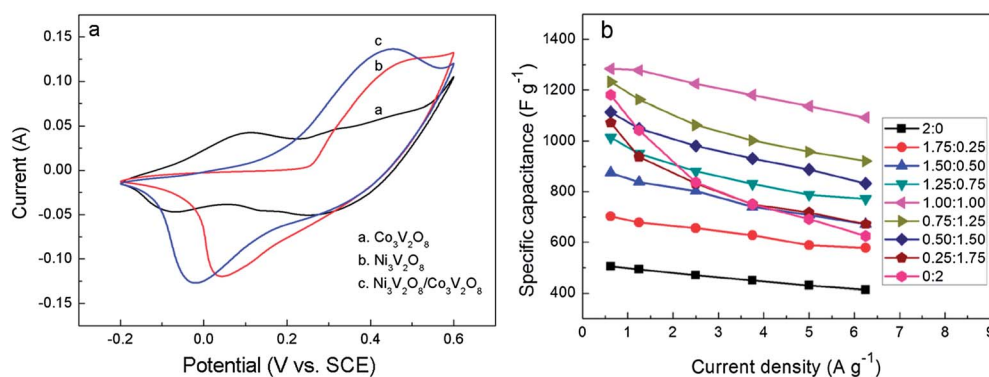


Fig. 6 (a) CV curves of  $\text{Ni}_3\text{V}_2\text{O}_8$ ,  $\text{Co}_3\text{V}_2\text{O}_8$ , and the  $\text{Ni}_3\text{V}_2\text{O}_8/\text{Co}_3\text{V}_2\text{O}_8$  composite with a Ni/Co molar ratio of 1 : 1. (b) The dependence of the specific capacitances on Ni/Co molar ratios.

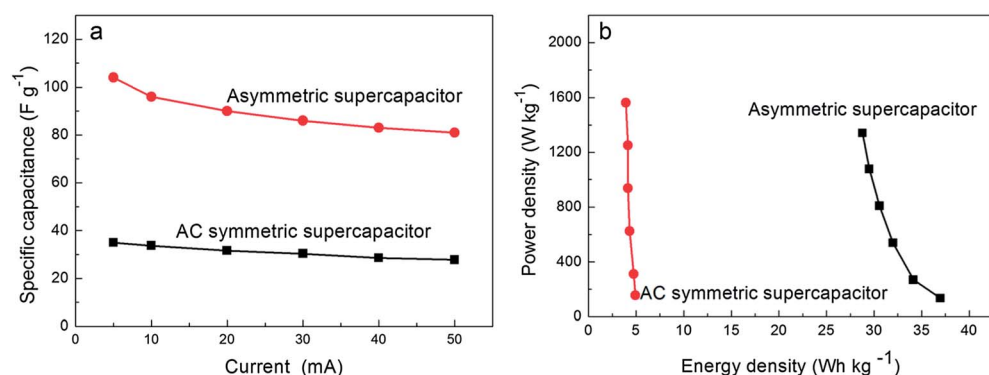


Fig. 7 (a) Specific capacitances and (b) Ragone plots of the assembled asymmetric supercapacitor and AC symmetric supercapacitor.



which indicates that the high capacitance of  $\text{Ni}_3\text{V}_2\text{O}_8$  noticeably improves the capacitances of the  $\text{Ni}_3\text{V}_2\text{O}_8/\text{Co}_3\text{V}_2\text{O}_8$  composites. The composite with a Ni/Co molar ratio of 1 : 1 shows the highest specific capacitance and the best rate capability; this value is also higher than that of bare  $\text{Ni}_3\text{V}_2\text{O}_8$  and  $\text{Co}_3\text{V}_2\text{O}_8$ , indicating a synergistic effect at this ratio. When the mass ratio further increases above 1 : 1, the specific capacitances of the composites are decreased and the rate capability is retained, suggesting that the rate capability of the composites is contributed by the  $\text{Co}_3\text{V}_2\text{O}_8$  component, while the high specific capacitances are ascribed to the  $\text{Ni}_3\text{V}_2\text{O}_8$  component.

For further evaluation of the properties of the  $\text{Ni}_3\text{V}_2\text{O}_8/\text{Co}_3\text{V}_2\text{O}_8$  composites, an asymmetric supercapacitor was assembled using  $\text{Ni}_3\text{V}_2\text{O}_8/\text{Co}_3\text{V}_2\text{O}_8$  as the positive electrode and activated carbon (AC) as the negative electrode. The CV curves, charge–discharge curves, and cycling performance of the asymmetric supercapacitor are shown in Fig. S7.† Fig. 7 shows the specific capacitances and Ragone plots of the assembled supercapacitor. The specific capacitances of the asymmetric supercapacitor are higher than that of the AC symmetric supercapacitor, which reveals that the application of the  $\text{Ni}_3\text{V}_2\text{O}_8/\text{Co}_3\text{V}_2\text{O}_8$  electrode as a positive electrode can improve the specific capacitances of the supercapacitor. In addition, the potential window of the asymmetric supercapacitor (1.6 V) is also higher than that of the AC based symmetric supercapacitor (1.0 V) in aqueous electrolytes. On the basis of the larger potential window and higher specific capacitances, the asymmetric supercapacitor exhibits superior energy density to the AC symmetric supercapacitor.

## 4. Conclusions

In summary, we have demonstrated the design and fabrication of  $\text{M}_3\text{V}_2\text{O}_8$  (M = Ni or Co) based nanostructures as a new family of electrode materials for high performance pseudocapacitors; the study confirmed that binary metal oxides ( $\text{A}_x\text{B}_y\text{O}_z$ ) with a higher atom proportion of A exhibit a higher pseudocapacitance. The prepared flake-like  $\text{Ni}_3\text{V}_2\text{O}_8$  possesses a high specific capacitance while the particle-like  $\text{Co}_3\text{V}_2\text{O}_8$  exhibits an excellent rate capability and cycle stability. To combine the pseudocapacitive advantages of both  $\text{Ni}_3\text{V}_2\text{O}_8$  and  $\text{Co}_3\text{V}_2\text{O}_8$ , a  $\text{Ni}_3\text{V}_2\text{O}_8/\text{Co}_3\text{V}_2\text{O}_8$  composite was designed and prepared by growing  $\text{Co}_3\text{V}_2\text{O}_8$  nanoparticles on the surface of  $\text{Ni}_3\text{V}_2\text{O}_8$  nanoflakes. The composite provides an excellent combination of both  $\text{Co}_3\text{V}_2\text{O}_8$  and  $\text{Ni}_3\text{V}_2\text{O}_8$ , and exhibits superior electrochemical performances including ultrahigh specific capacitances, excellent rate capability, and exceptional cycle stability. The results also indicate that the high specific capacitance of the composite is contributed by  $\text{Ni}_3\text{V}_2\text{O}_8$ , while the excellent rate capability and cycle stability are attributed to the  $\text{Co}_3\text{V}_2\text{O}_8$  component. The excellent electrochemical properties of the composite are attributed to its unique microstructure, feasible oxidation states, high surface area, and synergistic effects between  $\text{Co}_3\text{V}_2\text{O}_8$  and  $\text{Ni}_3\text{V}_2\text{O}_8$ .

## Acknowledgements

This work was supported by the National Natural Science Foundation of China (no. 51362018, 21163010), the Key Project

of Chinese Ministry of Education (no. 212183), and the Natural Science Funds for Distinguished Young Scholars of Gansu Province (no. 1111RJDA012).

## References

- X. Huang, Z. Y. Zeng, Z. X. Fan, J. Q. Liu and H. Zhang, *Adv. Mater.*, 2012, **24**, 6348.
- P. Simon and Y. Gogotsi, *Nat. Mater.*, 2008, **7**, 845.
- J. R. Miller, R. A. Outlaw and B. C. Holloway, *Science*, 2010, **329**, 1637.
- D. Pech, M. Brunet, H. Durou, P. Huang, V. Mochalin and Y. Gogotsi, *Nat. Nanotechnol.*, 2010, **5**, 651.
- T. Brezesinski, J. Wang, S. H. Tolbert and B. Dunn, *Nat. Mater.*, 2010, **9**, 146.
- D. Wei, M. R. J. Scherer, C. Bower, P. Andrew, T. Ryhanen and U. Steiner, *Nano Lett.*, 2012, **12**, 1857.
- C. Liu, F. Li, L. P. Ma and H. M. Cheng, *Adv. Mater.*, 2010, **22**, E28.
- R. R. Salunkhe, K. Jang, S. W. Lee, S. Yu and H. Ahn, *J. Mater. Chem.*, 2012, **22**, 21630.
- W. Chen, Z. L. Fan, L. Gu, X. H. Bao and C. L. Wang, *Chem. Commun.*, 2010, **46**, 3905.
- J. Bae, M. K. Song, Y. J. Park, J. M. Kim, M. L. Liu and Z. L. Wang, *Angew. Chem., Int. Ed.*, 2011, **50**, 1683.
- X. H. Lu, G. M. Wang, T. Zhai, M. H. Yu, J. Y. Gan, Y. X. Tong and Y. Li, *Nano Lett.*, 2012, **12**, 1690.
- H. C. Chien, W. Y. Cheng, Y. H. Wang and S. Y. Lu, *Adv. Funct. Mater.*, 2012, **22**, 5038.
- B. Babakhani and D. G. Ivey, *Electrochim. Acta*, 2011, **56**, 4753.
- T. Y. Wei, C. H. Chen, H. C. Chien, S. Y. Lu and C. C. Hu, *Adv. Mater.*, 2010, **22**, 347.
- J. W. Lee, A. S. Hall, J. D. Kim and T. E. Mallouk, *Chem. Mater.*, 2012, **24**, 1158.
- M. C. Liu, L. B. Kong, C. Lu, X. M. Li, Y. C. Luo and L. Kang, *ACS Appl. Mater. Interfaces*, 2012, **4**, 4631.
- T. Kokubu, Y. Oaki, E. Hosono, H. S. Zhou and H. Imai, *Adv. Funct. Mater.*, 2011, **21**, 3673.
- J. P. Liu, J. Jiang, C. W. Cheng, H. H. Li, J. X. Zhang, H. Gong and H. J. Fan, *Adv. Mater.*, 2011, **23**, 2076.
- Y. Yang, D. Kim, M. Yang and P. Schmuki, *Chem. Commun.*, 2011, **47**, 7746.
- M. C. Liu, L. B. Kong, C. Lu, X. M. Li, Y. C. Luo, L. Kang, X. H. Li and F. C. Walsh, *J. Electrochem. Soc.*, 2012, **159**, A1262.
- B. Senthilkumar, K. V. Sankar, R. K. Selvan, M. Danielle and M. Manickam, *RSC Adv.*, 2013, **3**, 352.
- Y. Q. Wu, X. Y. Chen, P. T. Ji and Q. Q. Zhou, *Electrochim. Acta*, 2011, **56**, 7517.
- Q. F. Wang, B. Liu, X. F. Wang, S. H. Ran, L. M. Wang, D. Chen and G. Z. Shen, *J. Mater. Chem.*, 2012, **22**, 21647.
- X. Wang, X. D. Han, M. F. Lim, N. D. Singh, C. L. Gan, M. Jan and P. S. Lee, *J. Phys. Chem. C*, 2012, **116**, 12448.
- H. C. Chien, W. Y. Cheng, Y. H. Wang and S. Y. Lu, *Adv. Funct. Mater.*, 2012, **22**, 5038.
- G. Q. Zhang and X. W. Lou, *Adv. Mater.*, 2013, **25**, 976.

- 1 27 H. Jiang, J. Ma and C. Z. Li, *Chem. Commun.*, 2012, **48**, 4465.
- 28 M. C. Liu, L. Kang, L. B. Kong, C. Lu, X. J. Ma, X. M. Li and  
Y. C. Luo, *RSC Adv.*, 2013, **3**, 6472.
- 5 29 M. C. Liu, L. B. Kong, X. J. Ma, C. Lu, X. M. Li, Y. C. Luo and  
L. Kang, *New J. Chem.*, 2012, **36**, 1713.
- 30 M. C. Liu, L. B. Kong, C. Lu, X. M. Li, Y. C. Luo and L. Kang,  
*Mater. Lett.*, 2013, **94**, 197.
- 31 G. Lawes, A. B. Harris, T. Kimura, N. Rogado, R. J. Cava,  
A. Aharony, O. Entin-Wohlman, T. Yildirim, M. Kenzelmann,  
C. Broholm and A. P. Ramirez, *Phys. Rev. Lett.*, 2005, **95**, 087205.
- 10 32 D. F. Wang, J. W. Tang, Z. G. Zou and J. H. Ye, *Chem. Mater.*,  
2005, **17**, 5177.
- 33 Z. Z. He, J. Yamaura and Y. Ueda, *Cryst. Growth Des.*, 2008, **8**,  
799.
- 15 34 B. Zhaorigetu, W. Z. Li, R. Kieffer and H. Y. Xu, *React. Kinet.*  
*Catal. Lett.*, 2002, **75**, 275.
- 35 J. W. Lang, L. B. Kong, M. Liu, Y. C. Luo and L. Kang,  
*J. Electrochem. Soc.*, 2010, **157**, A1341.
- 20 36 M. S. Balathanigaimani, W. G. Shim, M. J. Lee, C. Kim,  
J. W. Lee and H. Moon, *Electrochem. Commun.*, 2008, **10**, 868.
- 37 M. C. Liu, L. B. Kong, P. Zhang, Y. C. Luo and L. Kang,  
*Electrochim. Acta*, 2012, **60**, 443.
- 25 38 X. Li, F. C. Walsh and D. Pletcher, *Phys. Chem. Chem. Phys.*,  
2011, **13**, 1162.
- 39 M. Fleischmann, K. Korinek and D. Pletcher, *J. Electroanal.*  
*Chem.*, 1971, **31**, 39.
- 40 R. S. Schrebler Guzman, J. R. Vilche and A. J. Arvia,  
*J. Electrochem. Soc.*, 1978, **125**, 1578.
- 41 P. M. Robertson, *J. Electroanal. Chem.*, 1980, **111**, 97.
- 42 X. H. Xia, J. P. Tu, Y. Q. Zhang, X. L. Wang, C. D. Gu,  
X. B. Zhao and H. J. Fan, *ACS Nano*, 2012, **6**, 5531.
- 5 43 F. Zhang, C. Z. Yuan, X. J. Lu, L. J. Zhang, Q. Che and  
X. G. Zhang, *J. Power Sources*, 2012, **203**, 250.
- 44 L. Q. Mai, F. Yang, Y. L. Zhao, X. Xu, L. Xu and Y. Z. Luo, *Nat.*  
*Commun.*, 2011, **2**, 381.
- 45 M. C. Liu, L. B. Kong, C. Lu, X. J. Ma, X. M. Li, Y. C. Luo and  
L. Kang, *J. Mater. Chem. A*, 2013, **1**, 1380.
- 10 46 J. S. Bonso, A. Rahy, S. D. Perera, N. Nour, O. Seitz,  
Y. J. Chabal, K. J. Balkus Jr, J. P. Ferraris and D. J. Yang,  
*J. Power Sources*, 2012, **203**, 227.
- 15 47 B. Saravanakumar, K. K. Purushothaman and G. Muralidharan,  
*ACS Appl. Mater. Interfaces*, 2012, **4**, 4484.
- 48 J. W. Lang, L. B. Kong, W. J. Wu, Y. C. Luo and L. Kang,  
*Chem. Commun.*, 2008, 4213.
- 49 C. Y. Cao, W. Guo, Z. M. Cui, W. G. Song and W. Cai, *J. Mater.*  
*Chem.*, 2011, **21**, 3204.
- 20 50 J. P. Liu, J. Jiang, C. W. Cheng, H. H. Li, J. X. Zhang, H. Gong  
and H. J. Fan, *Adv. Mater.*, 2011, **23**, 2076.
- 51 Y. Yang, D. Kim, M. Yang and P. Schmuki, *Chem. Commun.*,  
2011, **47**, 7746.
- 25 52 X. H. Lu, M. H. Yu, G. M. Wang, T. Zhai, S. L. Xie, Y. C. Ling,  
Y. X. Tong and Y. Li, *Adv. Mater.*, 2013, **25**, 267.